Phosphorylation of pICln by the autophagy activating kinase ULK1 regulates snRNP biogenesis and splice activity of the cell

Lea Marie Esser, Katharina Schmitz, Frank Hillebrand, Steffen Erkelenz, Heiner Schaal, Björn Stork, Matthias Grimmler, Sebastian Wesselborg, Christoph Peter

Suggested Citation:
Esser, L. M., Schmitz, K., Hillebrand, F., Erkelenz, S., Schaal, H., Stork, B., Grimmler, M., Wesselborg, S., & Peter, C. (2023). Phosphorylation of pICln by the autophagy activating kinase ULK1 regulates snRNP biogenesis and splice activity of the cell [OnlineRessource]. Computational and Structural Biotechnology Journal , 21, 2100–2109. https://doi.org/10.1016/j.csbj.2023.03.015

Computational and Structural Biotechnology Journal 21 (2023) 2100–2109

Contents lists available at ScienceDirect

Computational and Structural Biotechnology Journal

journal homepage: www.elsevier.com/locate/csbj

Research article

Phosphorylation of pICln by the autophagy activating kinase ULK1 regulates snRNP biogenesis and splice activity of the cell

Lea Marie Esser [a], Katharina Schmitz [a], Frank Hillebrand [b], Steffen Erkelenz [b], Heiner Schaal [b], Björn Stork [a], Matthias Grimmler [c,1], Sebastian Wesselborg [a], Christoph Peter [a,*]

[a] Institute of Molecular Medicine I, Medical Faculty, Heinrich Heine University Düsseldorf, Düsseldorf, Germany
[b] Institute of Virology, University Hospital Düsseldorf, Düsseldorf, Germany
[c] HOCHSCHULEN FRESENIUS gem. Trägergesellschaft mbH, University of Applied Sciences, Limburger Straße 2, 65510 Idstein, Germany

ARTICLE INFO

Article history:
Received 15 September 2022
Received in revised form 10 March 2023
Accepted 11 March 2023
Available online 16 March 2023

Keywords:
Autophagy
PRMT5
pICln
ULK1
UsnRNP
spliceosomal activity

ABSTRACT

The spliceosome, responsible for all mature protein-coding transcripts of eukaryotic intron-containing genes, consists of small uridine-rich nuclear ribonucleoproteins (UsnRNPs). The assembly of UsnRNPs depends, on one hand, on the arginine methylation of Sm proteins catalyzed by the PRMT5 complex. On the other hand, it depends on the phosphorylation of the PRMT5 subunit pICln by the Uncoordinated Like Kinase 1 (ULK1). In consequence, phosphorylation of pICln affects the stability of the UsnRNP assembly intermediate, the so-called 6 S complex. The detailed mechanisms of phosphorylation-dependent integrity and subsequent UsnRNP assembly of the 6 S complex *in vivo* have not yet been analyzed.

By using a phospho-specific antibody against ULK1-dependent phosphorylation sites of pICln, we visualize the intracellular distribution of phosphorylated pICln. Furthermore, we detect the colocaliphosphor-pICln1 with phospho-pICln by size-exclusion chromatography and immunofluorescence techniques. We also show that phosphorylated pICln is predominantly present in the 6 S complex. The addition of ULK1 to *in vitro* produced 6 S complex, as well as the reconstitution of ULK1 in ULK1-deficient cells, increases the efficiency of snRNP biogenesis. Accordingly, inhibition of ULK1 and the associated decreased pICln phosphorylation lead to accumulation of the 6 S complex and reduction in the spliceosomal activity of the cell.

1. Introduction

Pre-mRNA splicing in eukaryotes is catalyzed by the spliceosome, a multimegadalton complex comprised of five small uridine-rich nuclear ribonucleoproteins (UsnRNPs) [1,2]. Each UsnRNPs consists of a specific UsnRNA (U1, U2, U4, U5, or U6) and, except for the U6 snRNP, a common set of seven Sm proteins (B, D1, D2, D3, E, F, and G), which form a ring-shaped structure around the UsnRNA and thus form the functional snRNP [1,3]. The assembly of Sm proteins and their respective snRNAs is mainly arranged by the cooperated action of two multiprotein complexes: the PRMT5 (Protein arginine N-methyltransferase 5), also called methylosome, and the SMN (Survival of motor neuron) complex [4–9]. The PRMT5 complex, consisting of the Protein Arginine Methyltransferase 5 (PRMT5), the WD-repeat protein WD45, and pICln, catalyzes the arginine methylation of the Sm proteins B, D1, and D3 and subsequently transfers them onto the SMN complex [4,8–10]. The SMN multiprotein complex consists of the survival of motor neuron (SMN) protein, its binding partners known as Gemins 2–8, and the UNR interacting protein (UNRIP) [5,11–15]. The SMN protein and Gemin2 form the functional core of the SMN complex that is responsible for binding the Sm proteins [15–17]. The interaction of the PRMT5 and the SMN multiprotein complexes in the assembly of snRNPs is a tightly regulated process in which pICln attributes a key role: on the one hand it recruits the Sm proteins as substrates for PRMT5 and on the other hand it also functions as an assembly chaperone by forming a stable ring-shaped RNA-free intermediate with the Sm proteins D1, D2, E, F, and G. This structure is called the 6 S complex [18,19]. To form functional snRNP, pICln must be released from this intermediate 6 S ring structure and needs to be replaced by the two missing Sm proteins B and D3. It has been speculated that this key substitutional step may be regulated by phosphorylation processes

* Corresponding author.
E-mail address: christoph.peter@uni-duesseldorf.de (C. Peter).
[1] Present address: DiaSys Diagnostic Systems GmbH, Holzheim, Germany

https://doi.org/10.1016/j.csbj.2023.03.015

[18]. In our recent work, we have shown that the autophagy activating Ser/Thr Unc-51-like kinase (ULK1) catalyzes the phosphorylation of specific serine residues of pICln in its C-terminus and mediates the release of Sm Proteins onto the SMN complex upon phosphorylation [20].

In our work presented here, we focus on the characterization of the phospho-status and cellular distribution of endogenous pICln and its influence on the efficiency of new synthesis of UsnRNPs, by using a phospho-pICln-specific antibody. We also address the subsequent ULK1-mediated /phospho-pICln-specific spliceosomal activity *in vivo*.

2. Experimental procedures

2.1. Antibodies

The following primary antibodies were used for immunoblotting and immunofluorescence: α-pICln C5 (sc-130668, Santa Cruz, mouse), Antibody recognizing phosphorylated pICln generated by Eurogentec (rabbit), Antibody recognizing pICln has been described previously (21, rabbit), α-SMN (05–1532, Merck, mouse), α-SmE (NBP243792, Novus Biologicals, rabbit), α-SmF (SAB2102258, Sigma Aldrich, rabbit), α-SmG (PA5–49365, Invitrogen, rabbit), α-SmD1 (AV40693, Sigma Aldrich, rabbit), α-SmD2 (SAB2102257, Sigma Aldrich, rabbit), α-2,2,7-Trimethylguanosin (MABE302, Merck, mouse), α-ULK1 (8054; CST, rabbit), α-ULK1 (HPA063990; Prestige Antibodies Sigma Aldrich, rabbit), α-ULK1 F4 (sc-390904; Santa Cruz, mouse). The detection of proteins was carried out with the following fluorescent secondary antibodies: IRDye 680LT goat α-rabbit, IRDye 680LT goat α-mouse, IRDye 800CW donkey α-rabbit, IRDye 800CW donkey α-mouse. For the detection of proteins *in vivo via* IF the following secondary antibodies were used: Goat anti-Mouse IgG (H+L) Cross-Adsorbed Secondary Antibody, Alexa Fluor 488 (A11001, Invitrogen), Donkey anti-Rabbit IgG (H+L) Highly Cross-Adsorbed Secondary Antibody, Alexa Fluor 647 (A31573, Invitrogen).

2.2. Plasmids and proteins

ULK1/2 inhibitor MRT67307 was obtained through the MRC PPU Reagents and Services facility (MRC PPU, College of Life Sciences, University of Dundee, Scotland, mrcppureagents.dundee.ac.uk).

For all *in vitro* assays, the used plasmids were described previously [20].

To analyze the influence of the ULK inhibition on the cellular splicing process, transient transfection with the following plasmids were used: SV SRSF2 (2X) SD1 Δvpuenv-eGFP, SV SRSF2 (2X) – 1G3U Δvpuenv-eGFP (for cloning strategy see [21,22]); pUCBΔU1, pUCU1 6 A (for cloning strategy see [21]). pXGH5 expressing the human growth hormone 1 (hGH1) under control of the mouse metallothionein-1 promoter was co-transfected for normalization and to monitor transfection efficiencies.

2.3. Cell lines and cell culture

All cells were cultivated at 37 °C, 5% CO_2 in a humidified area in Dulbecco´s Modified Eagle Medium (4,5 g/L D-glucose, 41965–039, Gibco) supplemented with 10% (v/v) Fetal Bovine Serum (FCS) (F0804, Sigma Aldrich), 100 U/ml Penicillin and 100 µg/ml Streptomycin (15140–122, Sigma Aldrich). HEK293T cells for immunofluorescence were seeded one day before the treatment with 1×10^5 per well. For knockdown of ULK1 for immunofluorescence analysis, HEK293T cells were transfected in 24-well plates using DharmaFECT1 (T-2001–02, GE Dharmacon) with 50 nM ULK1 siRNA (L-005049–00–0010, SMARTpool, ON-TARGETplus, GE Dharmacon) or 50 nM of the On-TARGET plus Non-targeting Control Pool (D-001810–10–20, GE Dharmacon) for 72 h. For inhibition of ULK1 in immunofluorescence analysis, cells were pre-incubated for 5 h with 30 µM ULK1 inhibitor MRT67307. For splicing assays, HEK293T cells were seeded in six-well plates with 2.5×10^5 cells per well. Before transfection, cells were pre-incubated for three hours with 30 µM of the ULK inhibitor MRT67307. Transient transfection was carried out by using the TransIT-LT1 reagent (Mirus Bio LLC) following the manufacturer's instructions and described previously [23]. Cells were harvested for total RNA isolation 20 h after ULK inhibitor addition. MEF ULK1/DKO cells were reconstituted as described before [20].

2.4. Protein expression and purification

Recombinant proteins were overexpressed in BL21 competent *E. coli* at RT for 4 h after induction with 1 mM IPTG. For cell lysis, the lysis buffer containing 300 mM NaCl, 50 mM Tris/HCl pH 7.5, 5 mM EDTA, 5 mM EGTA, 0.01% (v/v) Igepal, protease inhibitor cocktail (4693132001, Roche), 50 mg/ml Lysozyme (12650–88–3, Serva) was used as well as sonication. After centrifugation at 15,000 rpm for 1 h, the lysate was incubated with Glutathione-Sepharose 4B (17–0756–01, Cytivia) for 1.5 h at 4 °C and subsequently washed 3 times with lysis buffer before use in *in vitro* assays.

2.5. Cytoplasm extraction (S100) and size exclusion chromatography

HEK293T cells were incubated with Roeder A buffer [24] in three times cell volume for 10 min at room temperature, dounced 10 times with a tight douncer, and adjusted to a NaCl concentration of 150 mM. After centrifugation at 13,000 rpm for 30 min, the supernatants (S100 extracts) were filtrated with Millex-HA, 0.45 µm filter unit (Merck Millipore) and either used for immunopurification or applied to a Superdex 200 HiLoad 16/600 or Superdex 200 increase 10/300 GL column (GE Healthcare). For size exclusion chromatography 1 ml of the sample was fractionated in running buffer (150 mM NaCl, 50 mM Tris/HCl pH 7.5) and 0.5 ml fractions were collected and analyzed by immunoblotting. The columns were calibrated with thyroglobulin (669 kDa), ferritin (440 kDa), aldolase (158 kDa), and RNase (14 kDa) (GE Healthcare).

2.6. Immunoblotting and immunopurification

The protein concentration of S100 cytoplasm extract was measured by the Bradford method. The samples were separated by Tris/Tricine or Tris/Glycine SDS gel electrophoresis [25] and transferred to PVDF membranes (Immobilon-FL, Merck Millipore). For immunoblot analysis, indicated antibodies and signals were detected with an Odyssey LI-COR Imaging System. For endogenous immunopurification, Protein-G-Sepharose (GE17–0618–01, GE Healthcare) was coated with 1 µg of the specific antibody for 1 h rotating. Afterward, pre-cleared lysates were bound to the Sepharose for 3 h at 4 °C. Purified proteins were washed 3 times with washing buffer (50 mM Hepes-NaOH, pH 7.5, 150 mM NaCl, 1% Igepal, 2.5 mM $MgCl_2$, 0.8 U/µl RNase Inhibitor (N2611, Promega) and protease inhibitor cocktail (4693132001, Roche). The elution was obtained in sample buffer (375 mM Tris pH 7.5; 25.8% (w/v) glycerol; 12.3% (w/v) SDS; 0.06% (w/v) Bromophenol blue; 6% (v/v) β-mercaptoethanol; pH 6.8) and analyzed by immunoblotting.

2.7. Immunofluorescence microscopy

For Immunofluorescence 1×10^5 HEK293T cells per well were seeded on coverslips in 24-well plates in a humidified area at 37 °C, 5% CO_2 in Dulbecco´s Modified Eagle Medium (4.5 g/L D-glucose, 41965–039, Gibco) supplemented with 10% (v/v) FCS (F0804, Sigma Aldrich), 100 U/ml Penicillin and 100 µg/ml Streptomycin (15140–122, Sigma Aldrich) one day before staining. On the next day,

cells were fixed with 4% paraformaldehyde for 10 min and permeabilized with 0,2% Triton X-100, after these steps cells were washed three times with Dulbecco´s phosphate-buffered saline (DPBS, 14190–094, Gibco). Blocking of the cells was carried out with 5% BSA for 1 h at RT. For detection of pICln total, (both antibodies 1:500), phospho-specific pICln (1:500), and ULK1 total (both antibodies 1:500) cells were incubated for 2 h. For colocalization experiments with pICln-phospho, which is an antibody with rabbit host, and ULK1 F4 (sc-390904) antibody, which is a mouse host, were co-stained. For comparison as a control pICln total antibody from also rabbit host was used. To control whether ULK1 siRNA worked and if the inhibition or knockdown of ULK1 total has an effect on pICln total localization the following antibodies were used: ULK1 Prestige Antibody Sigma (HPA063990) rabbit host and pICln C5 antibody Santa Cruz mouse host (sc-130668). For immunofluorescence quantification pICln phospho/total the pICln C5 antibody was co-stained with the phospho-specific one. The secondary Alexa Fluor 488 and Alexa Fluor 647 antibodies were incubated for 1 h and the DNA was stained with DAPI. Microscopy was carried out with an Axio Observer microscope from Zeiss with an ApoTome.2 and a 40 x oil immersion objective.

2.8. Immunofluorescence quantification with Fiji

For the quantification of the intensity ratio between phospho-specific pICln and pICln total, a macro was written in Fiji software which measured the intensity of pICln total and pICln phospho in the area of each cell. Therefore, the macro recognized pICln total staining which is distributed all over the cell as the area of the cell, and the DAPI staining as the area of the nucleus. The total area of the cell was divided by the total DAPI count per picture which in consequence is the relative area of the cell per picture. Subsequently, the measured intensity for pICln total and phospho-specific pICln each was divided by the relative area of the cell which results in the relative fluorescence intensity of those two stainings per cell. For calculation, the value of the pICln phospho signal per cell was normalized on the value of the pICln total. Afterward, the values for MRT67307 treatment were normalized on HEK wt value, and the values for ULK1 siRNA were normalized on Non-targeting control. For every condition at least 300 cells were analyzed. The diagram and the calculation of the standard deviation as well as the statistics were made in Origin Software. To test the significance of the values the data were analyzed using a Mann-Whitney U test where the p value was below 0.005, meaning that the samples were significantly different from each other.

2.9. In vitro translation and interaction assay

The proteins were [^{35}S] methionine-labelled (Hartmann Analytic) by using the TNT Quick Coupled Transcription/Translation System (Promega). For interaction assay *in vitro* translated proteins were incubated with GST fusion proteins purified with Glutathione-Sepharose 4B (17–0756–01, Cytivia) rotating for 1.5 h at 4 °C in interaction buffer (300 mM NaCl, 50 mM Tris/HCl pH 7.5, 1 mM EGTA, 1 mM EDTA, 1 mM DTT, and 0.01% (v/v) Igepal). The GST fusion proteins were washed 2 times with interaction buffer and eluted by adding sample buffer, following SDS-PAGE, coomassie staining, and autoradiography.

2.10. In vivo labelling

For *in vivo* labelling cells were seeded in six-well plates in DMEM (4.5 g/L D-glucose, 41965–039, Gibco) supplemented with 10% FCS (F0804, Sigma Aldrich) with a density of 1 × 10^6 cells per well. The cells were starved in media without methionine and cysteine (D0422, Sigma Aldrich) for 30 min. For the labelling cells were incubated with 100 µl media containing 10% dialyzed FCS, 20 mM Hepes pH 7,4, and 25 µCi/ml [^{35}S] methionine-label for 3.5 h at 37 °C. Afterward, cells were washed with DPBS (14190–094, Gibco) 3 times and the pellet was harvested for cell lysis. For cell lysis a buffer containing 50 mM Hepes-NaOH, pH 7.5, 150 mM NaCl, 1% NP-40, 2.5 mM $MgCl_2$, 0.8 U/µl RNase Inhibitor (N2611, Promega), and protease inhibitor cocktail (4693132001, Roche) was used. Endogenous immunopurification was done as described above and after the separation by SDS-PAGE followed by a coomassie staining the gels were dried and analyzed by autoradiography.

2.11. RNA-isolation and quantitative RT-PCR (qPCR)

Total RNA was collected and the mRNAs were reverse transcribed as described in [23] and [26]. Quantitative RT-PCR analysis was performed by using Precision 2 × real-time PCR MasterMix with SYBR green (Primerdesign, UK) using LightCycler 1.5 (Roche). For quantification of the spliced and unspliced mRNA species the following primer pairs were used: spliced: #3210 (5′-TGAGGAGGCTTT TTTGGAGG) and #3211 (5′-TTCACTAATCGAATGGATCTGTC), unspliced: #3210 and #640 (5′-CAATACTACTTCTTGTGGGTTGG). For normalization, primers #1224 (5′-TCTTCCAGCCTCCCATCAGCGTT TGG) and #1225 (5′-CAACAGAAATCCAACCTAGAGCTGCT) were used to monitor the expression of the hGH1-mRNA of the co-transfected pXGH5 plasmid.

3. Results

3.1. Characterization of the phosphorylation state of pICln

To investigate the phospho-status of pICln we generated a phospho-specific pICln antibody against phosphorylated peptides of the C-terminal region. The specificity of the phospho-pICln antibody was tested by Western blotting, using recombinant non-phosphorylated pICln wildtype (wt) and the phospho-deficient mutants 193, 196, 197 A and D as negative control and S100 cytoplasm extract as a positive control. As shown in Fig. 1A, the phospho-specific antibody only recognized pICln from the S100 extract and not the recombinant non-phosphorylated proteins. This is in clear contrast to a pan-pICln antibody. To verify the specificity of the phospho-specific antibody concerning phosphorylation sites within the C-terminus of pICln at the serines 193, 195, and 197, recombinant wt pICln and the two phospho-deficient mutants 193, 195, 197 A and 193, 195, 197D were subjected to a phosphorylation experiment with active ULK1 and non-radioactive ATP. As shown in Fig. 1B, the phospho-specific antibody recognizes only recombinant wt protein that is phosphorylated. The two pICln mutants, which cannot be phosphorylated by ULK1 in the C-terminus, gave no signal with the phospho-specific antibody (Fig. 1B).

To analyze endogenous pICln and the phospho-content of pICln, HEK293T wild-type cell lysate was separated by size exclusion chromatography, following immunoblot analysis using pan-specific and phospho-specific antibodies against pICln. Total pICln (represented in green color) is distributed in a wide range, whereas pICln, phosphorylated in its C-terminus (represented in red) is only detectable in the distinct molecular weight range from 400 kDa to 100 kDa, including the 6 S complex, the size of 158 kDa (Fig. 1C). In contrast, treatment of HEK293T wild-type cells with the inhibitor MRT67307 and the knockdown of ULK1 with siRNA (SD 1 G) resulted in a marked decrease in the intensity of the phosphoantibody signal in Western blot analyzes after size-exclusion chromatography (Fig. 1D-F). This observation indicates that phosphorylated endogenous pICln is part of the 6 S complex. Since we already have shown in previous work [20], that ULK1 is responsible for the specific phosphorylation of pICln within its C-terminus, we investigated the influence of ULK1 activity on the integrity of the 6 S complex.

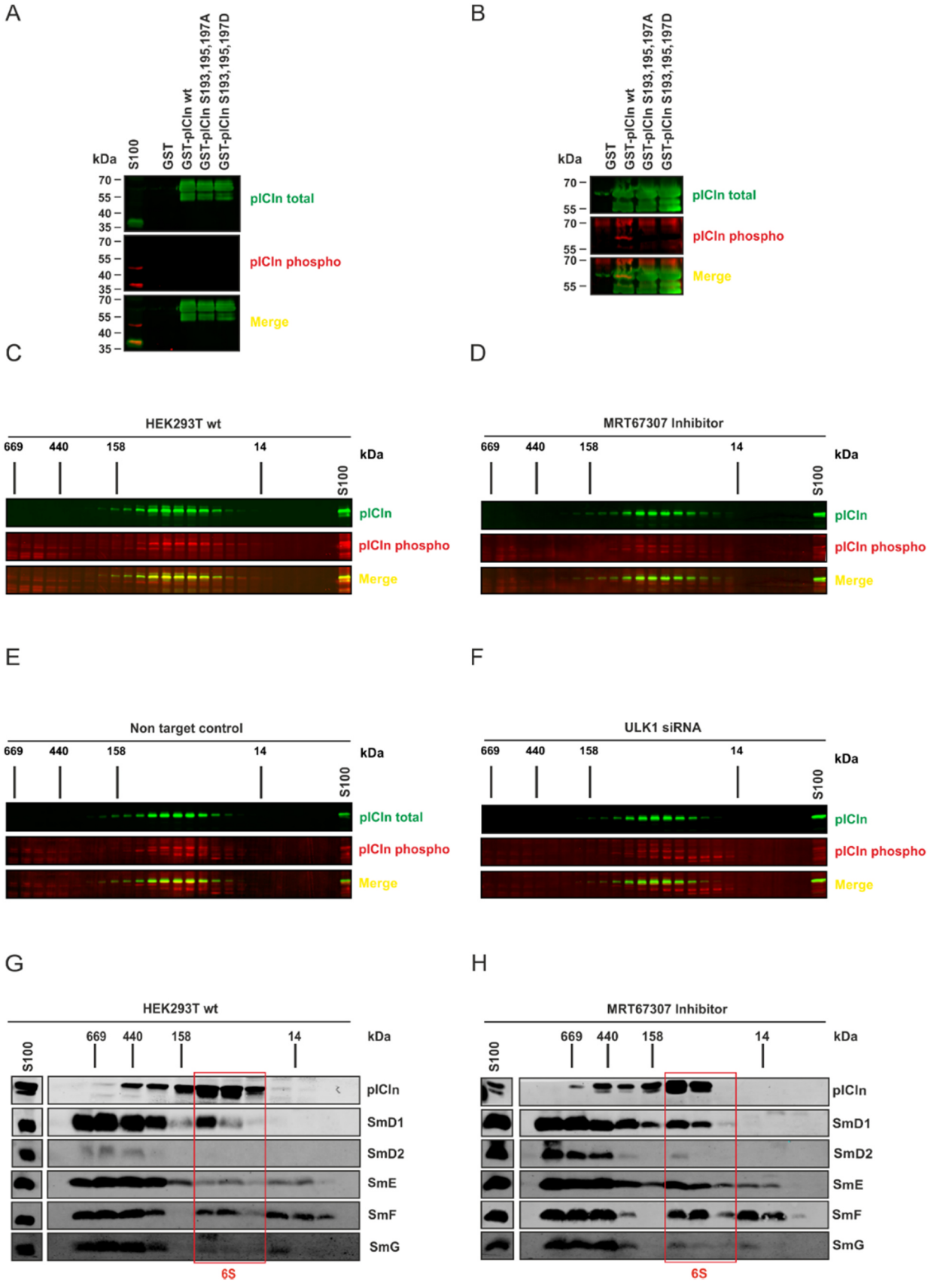

(caption on next page)

Fig. 1. Validation of pICln phosphorylation *in vitro* and *in vivo*. A, S100 extract of HEK293T cells and recombinant GST, GST-pICln wt, GST-pICln S193,195,197 A, and GST-pICln S193,195,197D were analyzed by Tris/Glycine-SDS-PAGE and western blotting using antibodies against phosphorylated pICln and total pICln. B, Recombinant GST, GST-pICln wt, GST-pICln S193,195,197 A, and GST-pICln S193,195,197D were incubated with 500 ng active GST-ULK1 and ATP for 1 h at 30 °C. The phosphorylation status of the proteins was analyzed by Tris/Glycine-SDS-PAGE and western blotting as described in A. C, D S100 extracts of untreated HEK293T cells or pre-treated cells (10 μM ULK inhibitor MRT67307) were generated with a douncer and applied to a Superdex 200 increase column. Fractions were analyzed by Tris/Glycine-SDS-PAGE and immunoblotting using antibodies against phosphospecific pICln and total pICln. E, F, HEK293T cells were transfected with 50 nM Non-targeting control pool (E) or ULK1 siRNA (F) for 72 h. The protein complexes of the S100 extract generated with a douncer were separated in a gel filtration with a Superdex 200 increase column. Protein complexes were analyzed by Tris/Glycine-SDS-PAGE and western blotting as described in C, D. G, H, HEK293T cells were treated with 10 μM ULK inhibitor MRT67307 for 1 h followed by S100 extraction and subsequent gel filtration using a Superdex 200 HiLoad 16/600 column. Obtained complexes were analyzed in comparison to untreated HEK293T cells by Tris/Tricine-SDS-PAGE and western blotting using antibodies against the Sm proteins. The 6 S complex is highlighted by the red box.

To test this scenario, we performed size exclusion chromatography with lysates of HEK293T cells, cultivated in the absence or presence of the inhibitor MRT67307 and detected the respective Sm proteins by immunoblotting. We observed an accumulation of SmD1/D2/E/F/G within the 6 S complex upon ULK1 inhibition (Fig. 1G, H; red box). On the one hand, these data show the composition and distribution of the entire endogenous 6 S for the first time. On the other hand, the data confirm that phosphorylation of pICln by ULK1 reduces the amount of the intracellular 6 S intermediate (Fig. 1G).

Using immunofluorescence analyses with the newly generated phospho-specific antibody against pICln and the ULK1-specific antibody, we next assessed the intracellular distribution and the interactions of pICln, phospho-pICln, and ULK1. Both total pICln and phospho-pICln co-localize with ULK1 predominantly in the cytoplasm. Total pICln signal intensity is significantly higher, compared to that of phospho-pICln (Fig. 2A). Knockdown of ULK1 by siRNA has no effect on the signal intensity of total pICln, nor has the inhibition of kinase activity by ULK-specific kinase inhibitor MRT67307 (Fig. 2B). However, the signal intensity of phosphorylated pICln significantly decreases upon both, inhibitor treatment and ULK1-knockdown (Fig. 2C). Relative to total pICln, there is a 40% reduction in phospho-pICln upon ULK1-knockdown and a 50% reduction after inhibitor treatment (Fig. 2D). This demonstrated, that in the cell, the phospho-status of pICln is directly regulated by ULK1.

Since we have previously shown [20], that the C-terminal phosphorylation of pICln by ULK1 regulates the binding properties of pICln to Sm proteins and thus snRNP biogenesis, we asked, whether phosphorylation of pICln affects the transfer efficiency of Sm proteins to the SMN complex.

To answer this question, we assessed the pICln-mediated transfer of ^{35}S-labelled reconstituted human 6 S complex onto immunopurified human SMN complex. Indeed, the 6 S complex sufficed for the transfer of the Sm proteins to the SMN complex. However, after treatment of the 6 S complex with recombinant active GST-ULK1 and ATP, the transfer rate of the Sm proteins is strongly enhanced (Fig. 3A and Supplemental Data (SD) 2 A). This finding indicated that ULK1-dependent phosphorylation of pICln enables a more efficient transfer of Sm proteins onto the SMN complex and is less involved in the turnover or degradation of pICln.

Because the SMN complex has a crucial role in the late assembly state of UsnRNPs we tested the consequence of ULK1-mediated phosphorylation of pICln to the late assembly machinery *in vivo*. To this end we performed metabolic labelling studies with [^{35}S] methionine in constitutive ULK1/ULK2-double knockout (DKO) MEF cells, individually reconstituting ULK1 or ULK2 only (Fig. 3B-E; SD 2B; C). Immunopurifications using an antibody specifically recognizing the m_3G/m^7G-cap of the snRNA, revealed that the Sm protein transfer onto the UsnRNA is dramatically reduced in ULK1 knockout cells in comparison to the corresponding vector control (Fig. 3D). Only MEF cells, reconstituted with ULK1 are capable to transfer Sm proteins onto UsnRNA to the same extent as the used control cells (Fig. 3D). This data confirms the crucial role of ULK1, but not the closely related kinase ULK2, in the UsnRNP assembly *in vivo*.

3.2. ULK1 regulates splice activity via enhanced snRNP biogenesis

To further investigate the influence of pICln phosphorylation on UsnRNP biogenesis *in vivo*, we analyzed the influence of ULK1 on subsequent U1 spliceosomal activity. Therefore, we pre-incubated HEK293T cells with the inhibitor MRT67307 and transfected them with the previously described splicing-reporter constructs [21,22]. These reporter constructs contain either a splice donor (D1) which is recognized by the endogenous U1 snRNA or the mutant splice donor site 3 U that requires co-expression of the complementary U1 6 A snRNA. Thus, co-transfection of the 3 U reporter and the U1 6 A snRNA expression vector allows for exclusive detection of the splicing activity which is dependent only on newly synthesized UsnRNPs (Fig. 4A).

To monitor the influence of ULK inhibition on the splicing of this specific reporter-construct derived RNAs, we performed qPCR analysis to determine the relative amount of spliced and unspliced mRNA of the respective constructs and calculated the spliced/unspliced mRNA ratio.

As expected, in the absence of the ULK inhibitor we observed predominantly spliced mRNA for both reporter constructs (90.9% for the D1 reporter and 86.9% for the 3 U reporter, when the U1 6 A snRNA was co-expressed) and a relatively small amount of unspliced mRNA (9.1% for the D1 and 13.1% for the 3 U reporter, when the U1 6 A snRNA was co-expressed) (Fig. 4B). In the absence of U1 6 A snRNA, we mainly detected unspliced mRNA when using the 3 U reporter (8.5% of spliced and 91.5% of unspliced mRNA) (Fig. 4B), demonstrating the requirement for of the U1 6 A snRNA expression. However, when cells were incubated with the ULK inhibitor MRT67307, we observed a substantially reduced spliced/unspliced ratio (Fig. 4C) with a decrease in spliced mRNA by 31.7% for the U1 6 A snRNA-dependent and 9.7% for the endogenous D1 splice site (Fig. 4B) with a concomitant increase in unspliced mRNA (Fig. 4B). These results clearly demonstrate that ULK inhibition reduces UsnRNP biogenesis and subsequent spliceosome activity *in vivo*.

4. Discussion

The Ser/Thr kinase ULK1 acts as a functional component of the PRMT5 complex by specific phosphorylation of pICln [20]. Here we characterize the phosphorylation status of endogenous pICln in depth, by using a phospho-specific antibody against the C-terminal, ULK1-specific phosphorylation sites of pICln. This allowed us to study the distribution of phospho-pICln at the endogenous level. Using immunofluorescence microscopy, it becomes evident, that phosphorylated pICln predominantly is detectable in the cytoplasm together with ULK1, and both methods, pharmacological inhibition or knockdown of ULK1 by siRNA led to a clear decrease in the signal intensity of phosphorylated pICln (Fig. 2D). However, originally developed as a ULK1/2 inhibitor [27], it turned out that the MRT67307 compound also inhibits TBK1 and IKKepsilon just as efficiently concerning kinase activities [28]. Both kinases have their main function predominantly in the immunological context or in immune cells [29]. Recently, however, it has been shown that TBK1/IKKepsilon also plays a role in energy metabolism and autophagy [30,31]. So far, we cannot exclude that TBK1 or IKKepsilon may have some

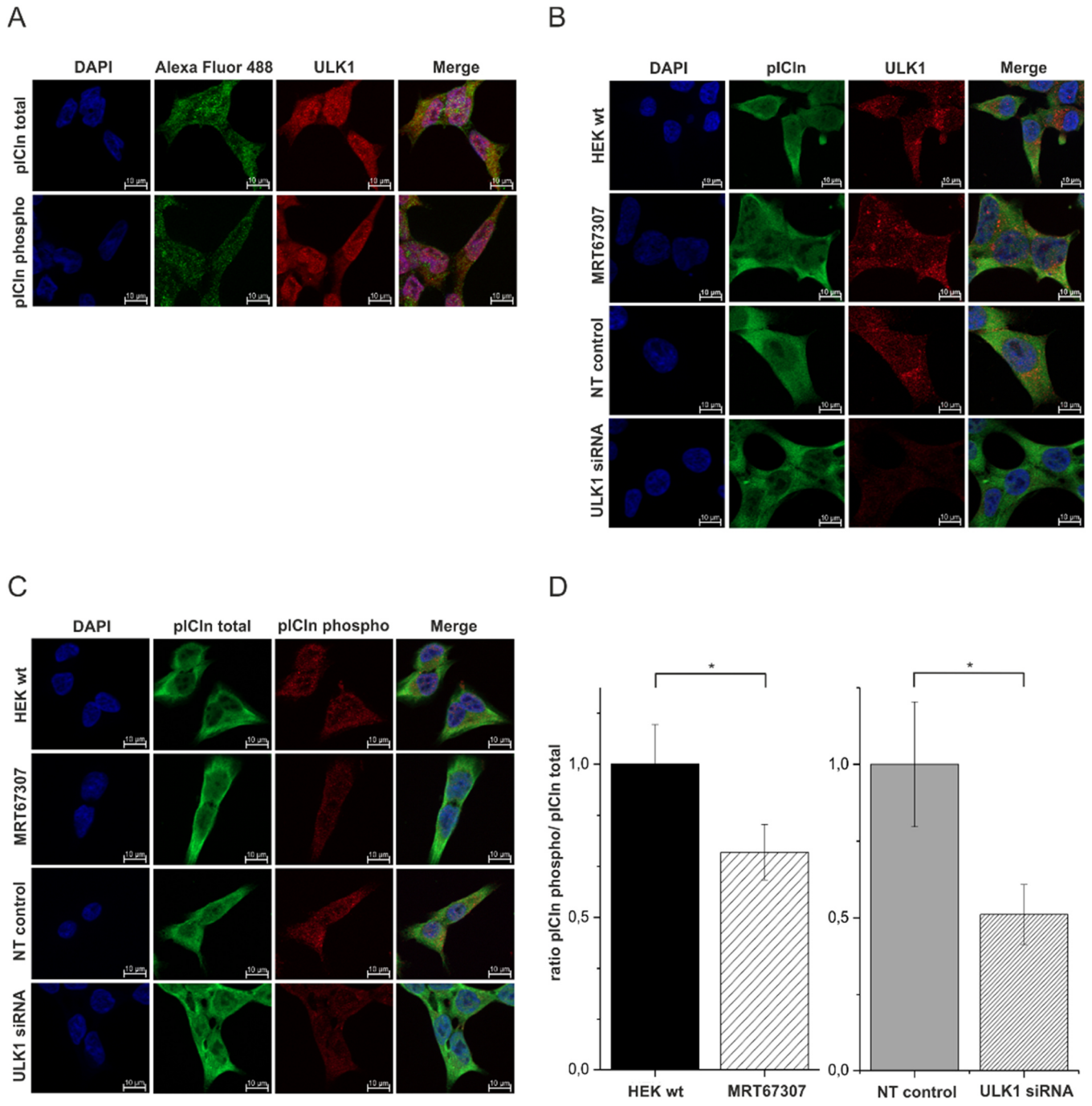

Fig. 2. Inhibition of ULK1 results in a decrease of pICln phosphorylation *in vivo* A, Colocalization of ULK1 and pICln phospho and total. Cells were fixed with 4% PFA and afterwards permeabilized with Triton X-100 to visualize ULK1 (red) and pICln total or phosphospecific pICln (green). The DNA was stained with DAPI (blue), scale bars 10 µm. B, HEK293T cells were treated with 30 µM ULK inhibitor MRT67307 for 5 h or transfected with 50 nM Non-targeting control pool (NT) control or ULK1 siRNA for 72 h. Cells were fixed as described in A to visualize ULK1 (red) and pICln total (green). The DNA was stained with DAPI (blue), scale bars 10 µm. C, HEK293T cells were treated as described in B to visualize phosphospecific pICln (red) and pICln total (green). The DNA was stained with DAPI (blue), scale bars 10 µm. **D,** Inhibition or knockdown of ULK1 decreases pICln phosphorylation *in vivo*. Quantification of the intensity ratio between phosphospecific pICln and pICln total was made in Fiji and the diagram in Origin, the values for MRT67307 treatment are normalized on HEK wt value, and the values for ULK1 siRNA are normalized on NT control. The significance of the values was analyzed using a Mann-Whitney U test, the p-value of HEK wt *vs.* MRT67307 and NT control *vs.* ULK1 siRNA was below 0.005, indicating significant differences between the values.

indirect influence on snRNP-biogenesis. It will be interesting in future work to investigate the role of both kinases in snRNP-biogenesis.

Our results are in line with the work of Sanchez-Olena et al. [32] and Grimmler and colleagues [33]. Both groups could independently show, that endogenous pICln is phosphorylated and a putative kinase activity can be detected on pICln immuno-purified from the cytoplasm. This suggests that pICln interacts with a kinase in the cytoplasm and is consequently phosphorylated.

Interestingly, the major amount of phosphorylated pICln is found in the size range around 158 kDa, which overlaps with the 6 S complex of Sm proteins (Fig. 1C; E). The intermediate 6 S complex plays a key role in UsnRNP biogenesis. The work by Chari and colleagues suggested, that the 6 S complex may be a kinetic trap, that is

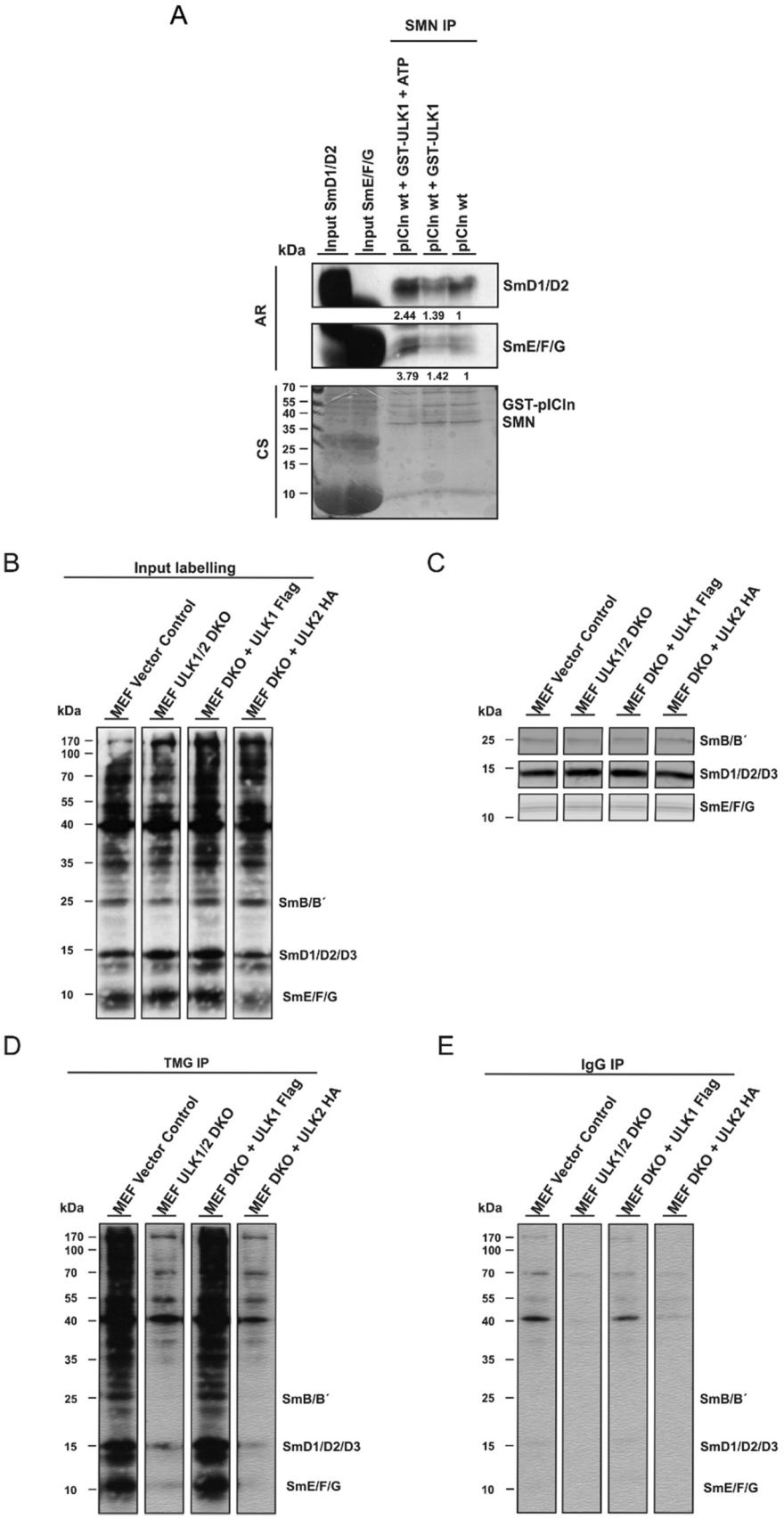

(caption on next page)

Fig. 3. ULK1 phosphorylation of pICln increases Sm protein transfer and late UsnRNP biogenesis A, pICln-mediated transfer of [^{35}S]-labelled reconstituted human 6 S complex onto immunopurified human SMN complex. To test the influence of ULK1 on the Sm protein transfer, immunopurified SMN complex was incubated with active GST-ULK1 with or without addition of ATP which increased the binding capacity of the SMN complex. B, As control of the metabolic labelling experiment, 10% of the [^{35}S] methionine lysate of ULK1/ULK2-double knockout MEF cells as well as individually reconstituted ones with Vector control. ULK1 Flag or ULK2 HA were analyzed by a Tris-Glycine SDS-PAGE and respective western blot. C, Whole cell lysate of MEF cells was analyzed by Tris/Glycine-SDS-PAGE and western blotting using antibodies against the Sm proteins for size comparison. D, Analysis of late assembly machinery *in vivo*. Therefore metabolic labelling with [^{35}S] methionine in constitutive ULK1/ULK2-double knockout MEF cells, individually reconstituting Vector control, ULK1 Flag, or ULK2 HA only was performed. After metabolic labelling immunopurification using an antibody recognizing the m_3G/m^7G-cap was performed. Only MEF cells reconstituted with ULK1 are capable to transfer Sm proteins onto UsnRNA to the same extent as MEF Vector control cells.

released by the phosphorylation of pICln to keep snRNP biogenesis ongoing [18]. Complementary to our previous work, in which we showed by *in vitro* binding studies, that ULK1 regulates the formation of the 6 S complex by phosphorylating pICln, our results show that pICln is largely phosphorylated in the 6 S complex.

Concordant with this data, one should expect that, when the kinase activity of ULK1 is inhibited, there should be an enrichment of the 6 S complex in the cell. This is indeed the case, as shown in Fig. 1G and H. Conversely, the transfer of Sm proteins to the SMN complex from the 6 S complex should be increased in the presence of ULK1. This is likewise the case (Fig. 3A, B), demonstrating that ULK1 activity is responsible for the equilibrium of endogenous 6 S complex-bound Sm proteins in the cytoplasm. Since snRNPs are the building blocks of the spliceosome [1,34], the influence of ULK1

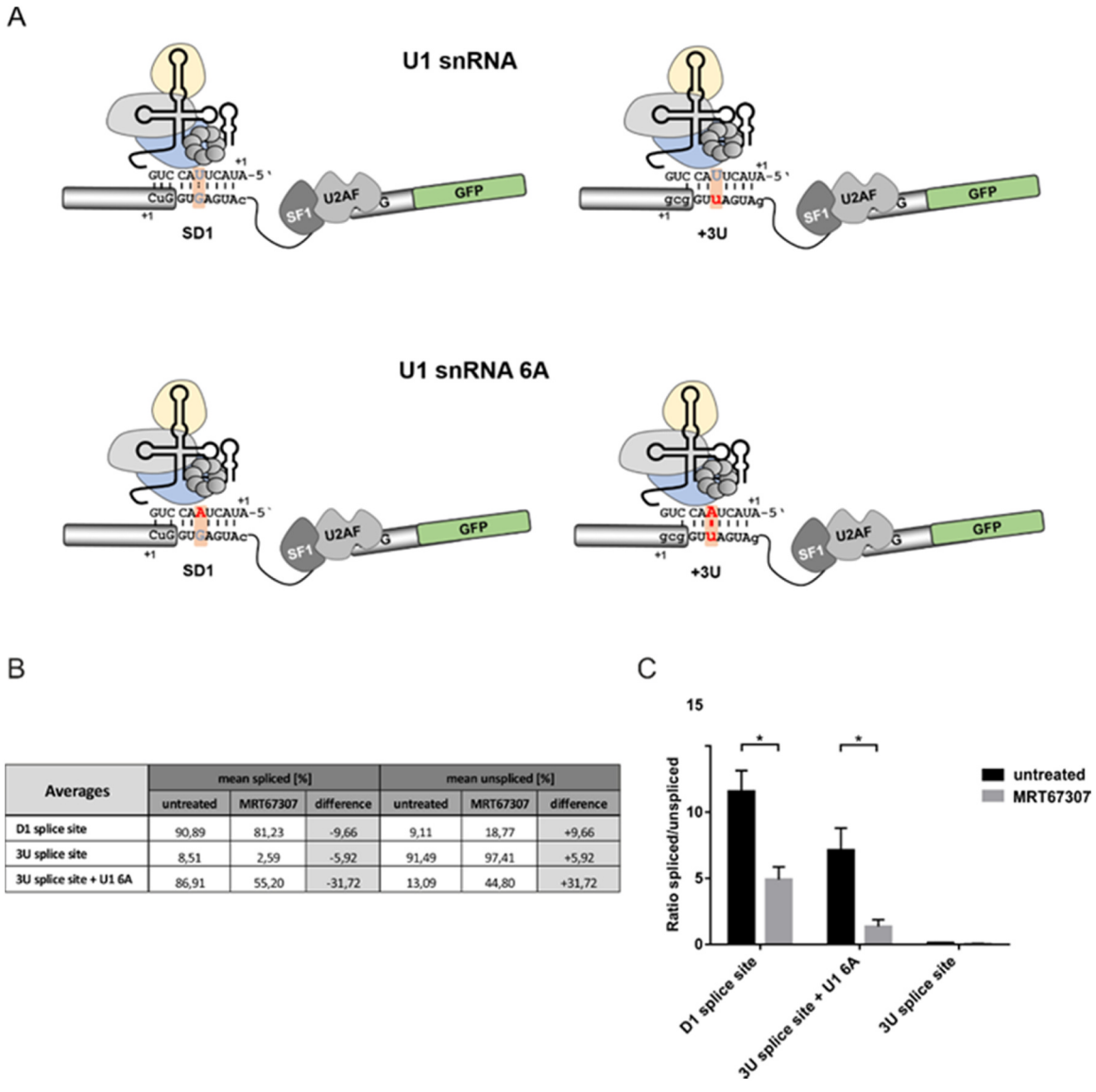

Averages	mean spliced [%]			mean unspliced [%]		
	untreated	MRT67307	difference	untreated	MRT67307	difference
D1 splice site	90,89	81,23	-9,66	9,11	18,77	+9,66
3U splice site	8,51	2,59	-5,92	91,49	97,41	+5,92
3U splice site + U1 6A	86,91	55,20	-31,72	13,09	44,80	+31,72

Fig. 4. ULK1 phosphorylation of pICln increases UsnRNP biogenesis and spliceosomal activity A, The HIV-1-based splicing reporter contains a test 5'splice site (5'ss) with a mutated version of viral 5′ss D4 termed „− 1G3U". This splice site carries two nucleotide substitutions: A-to-G at position − 1 (−1 G) and A-to-U at position + 3 (+3 U) and is poorly recognized by the endogenous U1 snRNA due to a mismatch at position + 3. However, splice site recognition is efficiently restored following the co-expression of a U1 snRNA with a compensatory U-to-A nucleotide exchange at position + 6, indicating that the modified U1 is assembled into functional snRNP particles within the cell. Uppercase letters within the splice site sequences represent complementary residues, while lowercase letters represent mismatches to the U1. Mutations are highlighted in red. Base-pairing at position + 3 is highlighted by a light red box and increased font size. B; C, HEK293T cells were treated with 30 μM inhibitor MRT67307 and transiently transfected with different splicing reporter constructs (see methods section for more details). After 20 h of inhibitor treatment cells were harvested to perform RNA isolation. Quantitative RT-PCR was executed and mRNA was analyzed by assessing the respective ratio of spliced/unspliced form, the p value was below 0.005 (B). The equal averages including differences between inhibitor-treated and untreated spliced and unspliced forms are listed in C (n = 3).

should also be reflected in the overall splice activity. We were also able to determine this by utilizing a splicing reporter assay (Fig. 4). In summary, it can be concluded that the interaction between ULK1 and pICln regulates snRNP biogenesis and consequently also influences subsequent splicing activity *in vivo*.

The crucial role of pICln in neurodegenerative diseases [35] and the unexpected link to ULK1, a key regulator of neurodifferentiation and axonal elongation in *C. elegans*, mice, and humans [36–38], make both, pICln as well as ULK1 to a new relevant target for further studies and potential therapies of SMA and other (motor) neuronal diseases. The successful introduction of antisense oligonucleotides (AONs) such as nusinersen [39] or gene replacement therapy [40], has dramatically increased the prospects for successful treatment of SMA patients. These novel treatments focus exclusively on increasing the protein levels of SMN. The long-term consequences caused by SMN overexpression are as yet unclear [41]. A simultaneous increase in snRNP biogenesis *via* activation of ULK1 could represent a new additional target for successful therapy. Much work will be necessary to gather more experimental data on this – but the association of pICln with ULK1 gives a new starting option on this so far blind alley to answer the question of why general spliceosomal defects predominantly do lead to neuronal manifestations.

Funding

This work was supported by grants from Deutsche Forschungsgemeinschaft [RTG 2158 (to B.S. and S.W.), RTG 2578 (to B.S. and S.W.), and STO 864/4-3 (to B.S.)] and the Düsseldorf School of Oncology (funded by the Comprehensive Cancer Center Düsseldorf/Deutsche Krebshilfe and the Medical Faculty of the Heinrich Heine University Düsseldorf; to B.S. and S.W.).

CRediT authorship contribution statement

L.E. performed *in vivo* labelling experiments as well as the Western blots of S100 extract of MEF cells, Western Blot analysis of recombinant pICln and pre-phosphorylated recombinant pICln, size exclusion with or without inhibitor-/ siRNA-treatment using the phospho-specific pICln antibody, immunofluorescence analysis and *in vitro* assembly assays; Ka.Sc. performed the gel filtrations with and without inhibitor treatment, and *in vitro* assembly assays; S.E., H.F., and H.S. performed and interpreted splicing analysis; B.S. and S.W. discussed the results; M.G. and C.P. designed the experiments and supervised the project; all authors contributed to the writing of the manuscript.

Declaration of Competing Interest

The authors declare that they have no known competing financial interests or personal relationships that could have appeared to influence the work reported in this paper.

Acknowledgments

We gratefully acknowledge Maximilian Jüdt, Qiaoping Li, David Schlütermann, Seda Akgün and Maria Jose Mendiburo for valuable discussions and technical support.

Appendix A. Supporting information

Supplementary data associated with this article can be found in the online version at doi:10.1016/j.csbj.2023.03.015.

References

[1] Matera AG, Wang Z. A day in the life of the spliceosome. Nat Rev Mol Cell Biol 2014;15:108–21.
[2] Maniatis T, Reed R. The role of small nuclear ribonucleoprotein particles in pre-mRNA splicing. Nature 1987;325:673–8.
[3] Kambach C, Walke S, Young R, Avis JM, de la Fortelle E, Raker VA, Luhrmann R, Li J, Nagai K. Crystal structures of two Sm protein complexes and their implications for the assembly of the spliceosomal snRNPs. Cell 1999;96:375–87.
[4] Meister G, Eggert C, Buhler D, Brahms H, Kambach C, Fischer U. Methylation of Sm proteins by a complex containing PRMT5 and the putative U snRNP assembly factor pICln. Curr Biol 2001;11:1990–4.
[5] Fischer U, Liu Q, Dreyfuss G. The SMN-SIP1 complex has an essential role in spliceosomal snRNP biogenesis. Cell 1997;90:1023–9.
[6] Liu Q, Fischer U, Wang F, Dreyfuss G. The spinal muscular atrophy disease gene product, SMN, and its associated protein SIP1 are in a complex with spliceosomal snRNP proteins. Cell 1997;90:1013–21.
[7] Buhler D, Raker V, Luhrmann R, Fischer U. Essential role for the tudor domain of SMN in spliceosomal U snRNP assembly: implications for spinal muscular atrophy. Hum Mol Genet 1999;8:2351–7.
[8] Meister G, Fischer U. Assisted RNP assembly: SMN and PRMT5 complexes cooperate in the formation of spliceosomal UsnRNPs. EMBO J 2002;21:5853–63.
[9] Friesen WJ, Paushkin S, Wyce A, Massenet S, Pesiridis GS, Van Duyne G, Rappsilber J, Mann M, Dreyfuss G. The methylosome, a 20S complex containing JBP1 and pICln, produces dimethylarginine-modified Sm proteins. Mol Cell Biol 2001;21:8289–300.
[10] Brahms H, Meheus L, de Brabandere V, Fischer U, Luhrmann R. Symmetrical dimethylation of arginine residues in spliceosomal Sm protein B/B′ and the Sm-like protein LSm4, and their interaction with the SMN protein. RNA 2001;7:1531–42.
[11] Selenko P, Sprangers R, Stier G, Buhler D, Fischer U, Sattler M. SMN tudor domain structure and its interaction with the Sm proteins. Nat Struct Biol 2001;8:27–31.
[12] Meister G, Buhler D, Pillai R, Lottspeich F, Fischer U. A multiprotein complex mediates the ATP-dependent assembly of spliceosomal U snRNPs. Nat Cell Biol 2001;3:945–9.
[13] Grimmler M, Otter S, Peter C, Muller F, Chari A, Fischer U. Unrip, a factor implicated in cap-independent translation, associates with the cytosolic SMN complex and influences its intracellular localization. Hum Mol Genet 2005;14:3099–111.
[14] Otter S, Grimmler M, Neuenkirchen N, Chari A, Sickmann A, Fischer U. A comprehensive interaction map of the human survival of motor neuron (SMN) complex. J Biol Chem 2007;282:5825–33.
[15] Kroiss M, Schultz J, Wiesner J, Chari A, Sickmann A, Fischer U. Evolution of an RNP assembly system: a minimal SMN complex facilitates formation of UsnRNPs in Drosophila melanogaster. Proc Natl Acad Sci USA 2008;105:10045–50.
[16] Zhang R, So BR, Li P, Yong J, Glisovic T, Wan L, Dreyfuss G. Structure of a key intermediate of the SMN complex reveals Gemin2's crucial function in snRNP assembly. Cell 2011;146:384–95.
[17] Veepaschit J, Viswanathan A, Bordonne R, Grimm C, Fischer U. Identification and structural analysis of the Schizosaccharomyces pombe SMN complex. Nucleic Acids Res 2021;49:7207–23.
[18] Chari A, Golas MM, Klingenhager M, Neuenkirchen N, Sander B, Englbrecht C, Sickmann A, Stark H, Fischer U. An assembly chaperone collaborates with the SMN complex to generate spliceosomal SnRNPs. Cell 2008;135:497–509.
[19] Fisher DE, Conner GE, Reeves WH, Wisniewolski R, Blobel G. Small nuclear ribonucleoprotein particle assembly in vivo: demonstration of a 6S RNA-free core precursor and posttranslational modification. Cell 1985;42:751–8.
[20] Schmitz K, Cox J, Esser LM, Voss M, Sander K, Loffler A, Hillebrand F, Erkelenz S, Schaal H, Kahne T, et al. An essential role of the autophagy activating kinase ULK1 in snRNP biogenesis. Nucleic Acids Res 2021;49:6437–55.
[21] Kammler S, Leurs C, Freund M, Krummheuer J, Seidel K, Tange TO, Lund MK, Kjems J, Scheid A, Schaal H. The sequence complementarity between HIV-1 5′ splice site SD4 and U1 snRNA determines the steady-state level of an unstable env pre-mRNA. RNA 2001;7:421–34.
[22] Erkelenz S, Mueller WF, Evans MS, Busch A, Schoneweis K, Hertel KJ, Schaal H. Position-dependent splicing activation and repression by SR and hnRNP proteins rely on common mechanisms. RNA 2013;19:96–102.
[23] Erkelenz S, Hillebrand F, Widera M, Theiss S, Fayyaz A, Degrandi D, Pfeffer K, Schaal H. Balanced splicing at the Tat-specific HIV-1 3'ss A3 is critical for HIV-1 replication. Retrovirology 2015;12:29.
[24] Dignam JD, Lebovitz RM, Roeder RG. Accurate transcription initiation by RNA polymerase II in a soluble extract from isolated mammalian nuclei. Nucleic Acids Res 1983;11:1475–89.
[25] Laemmli UK. Cleavage of structural proteins during the assembly of the head of bacteriophage T4. Nature 1970;227:680–5.
[26] Chomczynski P, Sacchi N. Single-step method of RNA isolation by acid guanidinium thiocyanate-phenol-chloroform extraction. Anal Biochem 1987;162:156–9.
[27] Petherick KJ, Conway OJ, Mpamhanga C, Osborne SA, Kamal A, Saxty B, Ganley IG. Pharmacological inhibition of ULK1 kinase blocks mammalian target of rapamycin (mTOR)-dependent autophagy. J Biol Chem 2015;290:11376–83.
[28] Saric A, Hipolito VE, Kay JG, Canton J, Antonescu CN, Botelho RJ. mTOR controls lysosome tubulation and antigen presentation in macrophages and dendritic cells. Mol Biol Cell 2016;27:321–33.
[29] Clark K, Peggie M, Plater L, Sorcek RJ, Young ER, Madwed JB, Hough J, McIver EG, Cohen P. Novel cross-talk within the IKK family controls innate immunity. Biochem J 2011;434:93–104.

[30] Chiang SH, Bazuine M, Lumeng CN, Geletka LM, Mowers J, White NM, Ma JT, Zhou J, Qi N, Westcott D, et al. The protein kinase IKKepsilon regulates energy balance in obese mice. Cell 2009;138:961–75.
[31] Reilly SM, Chiang SH, Decker SJ, Chang L, Uhm M, Larsen MJ, Rubin JR, Mowers J, White NM, Hochberg I, et al. An inhibitor of the protein kinases TBK1 and IKK-varepsilon improves obesity-related metabolic dysfunctions in mice. Nat Med 2013;19:313–21.
[32] Sanchez-Olea R, Emma F, Coghlan M, Strange K. Characterization of pICln phosphorylation state and a pICln-associated protein kinase. Biochim Biophys Acta 1998;1381:49–60.
[33] Grimmler M, Bauer L, Nousiainen M, Korner R, Meister G, Fischer U. Phosphorylation regulates the activity of the SMN complex during assembly of spliceosomal U snRNPs. EMBO Rep 2005;6:70–6.
[34] Newman AJ, Nagai K. Structural studies of the spliceosome: blind men and an elephant. Curr Opin Struct Biol 2010;20:82–9.
[35] Winkler C, Eggert C, Gradl D, Meister G, Giegerich M, Wedlich D, Laggerbauer B, Fischer U. Reduced U snRNP assembly causes motor axon degeneration in an animal model for spinal muscular atrophy. Genes Dev 2005;19:2320–30.
[36] Ogura K, Wicky C, Magnenat L, Tobler H, Mori I, Muller F, Ohshima Y. Caenorhabditis elegans unc-51 gene required for axonal elongation encodes a novel serine/threonine kinase. Genes Dev 1994;8:2389–400.
[37] Tomoda T, Bhatt RS, Kuroyanagi H, Shirasawa T, Hatten ME. A mouse serine/threonine kinase homologous to C. elegans UNC51 functions in parallel fiber formation of cerebellar granule neurons. Neuron 1999;24:833–46.
[38] Loh SH, Francescut L, Lingor P, Bahr M, Nicotera P. Identification of new kinase clusters required for neurite outgrowth and retraction by a loss-of-function RNA interference screen. Cell Death Differ 2008;15:283–98.
[39] Hoy SM. Nusinersen: first global approval. Drugs 2017;77:473–9.
[40] Mendell JR, Al-Zaidy S, Shell R, Arnold WD, Rodino-Klapac LR, Prior TW, Lowes L, Alfano L, Berry K, Church K, et al. Single-dose gene-replacement therapy for spinal muscular atrophy. New Engl J Med 2017;377:1713–22.
[41] Aslesh T, Yokota T. Restoring SMN expression: an overview of the therapeutic developments for the treatment of spinal muscular atrophy. Cells 2022:**11**.